Journal of Sound and Vibration (1993) **162**(1), 27–42

SOUND PROPAGATON IN NARROW TUBES OF ARBITRARY CROSS-SECTION

A. CUMMINGS

Department of Engineering Design and Manufacture, University of Hull, Hull, Humberside HU6 7RX, England

(*Received* 24 *June* 1991, *and in final form* 5 *November* 1991)

A variational treatment of the problem of sound transmission in narrow tubes is described as an alternative to the more usual analytical procedures, which are limited to mathematically tractable geometries. This method can be used for any cross-sectional geometry, as long as the cross-section of the tube is uniform along its length. Very simple low frequency and high frequency approximate solutions are obtained by the use of idealized trial functions, and these compare tolerably well to existing analytical solutions for a variety of geometries.

1. INTRODUCTION

The propagation of sound in a narrow tube containing a viscous, heat-conducting fluid is a topic that has attracted considerable interest over the years, mainly because of its generalization to the acoustics of porous media. The exact solution of Kirchhoff [1] and Rayleigh [2], for a tube of circular cross-section, has been examined by Zwikker and Kosten [3], who described a simplified treatment involving various approximations. Tijdeman [4] has examined these approximatons in some detail and presented numerical solutions to the exact Kirchhoff equations. Biot [5] and Smith and Greenkorn [6] (for example) have discussed the extension of a single tube model to a bulk porous medium, and introduced the idea of a "shape factor", relating the circular tube solution to that of a tube having an arbitrary cross-sectional shape. Attenborough [7] has discussed this question further, and highlighted the role of circular tubes and slits as extreme cases of cross-sectional geometry. Roh *et al.* [8] described a series solution for sound propagation in rectangular tubes. Stinson and Champoux [9, 10] reported an exact solution for tubes of equilateral triangular section and defined a new, frequency-independent, shape factor that is applicable at both low and high frequencies (the apparent need for a frequency-dependent "dynamic shape factor" had been evident in previous published work, for instance that of Attenborough [7]). It would seem that the geometries for which analytical solutions are available are restricted to circular, triangular and rectangular shapes. No doubt there are other configurations, such as the ellipse (the solutions for which would involve Mathieu functions) that could be treated by analytical means, but the range is clearly rather limited.

Craggs and Hildebrandt [11, 12] carried out a finite element analysis of sound propagation in tubes of arbitrary cross-section. They addressed themselves only to the solution to the velocity equation, however, making the assumption that the thermodynamic process involved in the wave motion was isothermal; this assumption is valid only at relatively low frequencies. Consequently, their results are of somewhat limited applicability, although their computed particle velocity contours and effective fluid density and flow resistivity provide a useful check on other methods of analysis.

0022-460X/93/070027+16 $08.00/0

Stinson [13] discussed the matter of sound propagation in both narrow and wide tubes, and derived low and high frequency approximations from the exact Kirchhoff solution. He also presented a "general procedure", applicable to tubes of arbitrary cross-sectional shape. The generality disappeared from his analysis, however, as soon as specific geometries had to be considered, and he restricted himself to circular and rectangular cross-sectional shapes in discussing applications. In finding solutions to the governing equations, one is still faced with limitations imposed by the co-ordinate system appropriate to the cross-sectional geometry of the tube, and the available solutions to the governing equations in that co-ordinate system.

These limitations are, of course, removed when a numerical solution (such as the finite element method) is adopted, but the penalty here is a certain loss of "feel" for the physics of the problem; certainly, it is difficult, from purely numerical results, to obtain approximations to the solution such as those discussed by Stinson [13] for low and high frequencies. A "halfway house" between exact solutions and numerical solutions is the sort of approximate result that may be obtained by the use of variational methods. Provided that we choose a trial function that bears a passing resemblance to the expected form of the exact solution (and this, of course, is open to speculation in cases in which no exact solution is known), we may obtain tolerably good results. The attractive feature of a simple variational solution is that it gives rise to mathematical expressions that may readily be interpreted in terms of appropriate physical aspects of the problem.

In this paper both low frequency and high frequency variational solutions are described for sound propagation in a narrow tube of axially uniform, arbitrary cross-section, containing a viscous, heat-conducting fluid at rest and with uniform properties. The results will be compared to other solutions for tubes having various cross-sectional shapes.

2. THEORY

2.1. GOVERNING EQUATIONS AND BOUNDARY CONDITIONS

The transverse velocity components in the tube may be shown to be relatively small compared to the axial component for narrow tubes at sufficiently low frequencies and, in the linearized Navier–Stokes equation for axial components, the terms containing the divergence of the particle velocity and the second axial derivative of the axial velocity are also negligible (see, for example, the paper by Stinson [13] for justification of these assumptions, and also that by Cummings and Chang [14]). This equation may thus be written in the approximate form

$$\mu \nabla_t^2 u - \bar{\rho}\, \partial u/\partial t = \partial p/\partial x \tag{1a}$$

(see Figure 1), where μ is the coefficient of dynamic viscosity, $\bar{\rho}$ is the fluid density, u is the axial particle velocity, p is the pressure perturbation (assumed to be uniform across

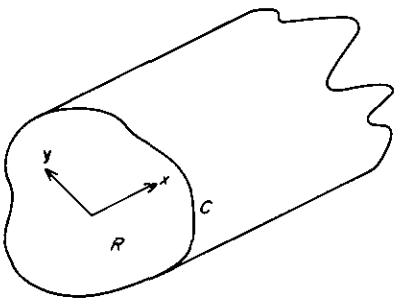

Figure 1. A uniform tube of arbitrary cross-sectional shape.

the tube) and ∇_t^2 is the Laplacian operator on the cross-section of the tube. If one takes p and u to be proportional to $\exp[i(\omega t - \alpha x)]$, ω being the radian frequency and α the axial wavenumber, then equation (1a) becomes

$$(\nabla_t^2 - i\omega/\nu)u = (-i\alpha/\mu)p, \tag{1b}$$

where ν is the kinematic viscosity coefficient of the fluid.

In the linearized energy equation, if the second axial derivative of the temperature perturbation T is discarded as being negligibly small compared to $\nabla_t^2 T$, then this equation may be written as

$$K\nabla_t^2 T - \bar{\rho} C_p \, \partial T/\partial t = -\partial p/\partial t, \tag{2a}$$

where C_p is the specific heat of the gas at constant pressure and K is the thermal conductivity. *A priori*, one may write equation (2a) as

$$(\nabla_t^2 - i\omega\bar{\rho} C_p/K)T = (-i\omega/K)p. \tag{2b}$$

Stinson [13] has pointed out that equations (1b) and (2b) are isomorphic. Furthermore, the boundary conditions imposed in this problem are the same in both equations, viz., u and T are both zero on C, the tube boundary (since it is assumed that the particle velocity must be zero at a solid boundary, and that the thermal capacity of the tube wall is such that the temperature is constant at the wall). Stinson therefore wrote the two equations in the form

$$(\nabla_t^2 - i\omega/\eta)\psi = -i\omega/\eta, \tag{3}$$

where $\psi = (\omega\bar{\rho}/\alpha p)u$, $\eta = \nu$ in the velocity equation, $\psi = (\bar{\rho} C_p/p)T$, $\eta = \nu/Pr$ in the temperature equation and Pr is the Prandtl number of the gas. A function $F(\eta)$ is defined as $\langle\psi\rangle$, the average of ψ over R (the tube cross-section), and then the axial wavenumber is given by the expression

$$\alpha = (\omega/c)\{[\gamma - (\gamma - 1)F(\nu/Pr)]/F(\nu)\}^{1/2}, \tag{4}$$

where c is the adiabatic sound speed in the gas.

The problem now is to solve equation (3) on the cross section of the tube, subject to the boundary condition $\psi = 0$ on C. The resulting solutions for ψ yield the distribution of the axial particle velocity or temperature perturbation (as the case may be) on the cross-section of the tube. From a combination of both these solutions one finds the axial wavenumber α by the use of equation (4), and one also can note that

$$\text{axial attenuaton rate } \Lambda \text{ (dB/unit distance)} = -8{\cdot}6858 \operatorname{Im}(\alpha), \tag{5a}$$

$$\text{phase speed } c_p = \omega/\operatorname{Re}(\alpha). \tag{5b}$$

2.2. VARIATIONAL FORMULATION

If $\psi = \Psi(y)\exp[i(\omega t - \alpha x)]$, one may define a functional $\Phi(\Psi)$ as

$$\Phi = (1/2)\int\int_R [\nabla_t\Psi \cdot \nabla_t\Psi + (i\omega/\eta)\Psi^2 - (i2\omega/\eta)\Psi]\, dR. \tag{6}$$

By putting $\delta\Phi = 0$ and using Green's formulae, it readily may be shown that the Euler equations for Φ are the governing differential equation (3) and the natural boundary condition $\nabla\Psi \cdot \mathbf{n} = 0$, $\mathbf{n}$ being the outward unit normal from R, on C (see, for example, the book by Zienkiewicz and Taylor [15] for a discussion of variational techniques). This natural boundary condition is not, in fact, the appropriate physical boundary condition

($\Psi = 0$ on C) which must, therefore, be imposed as a forced boundary condition. This procedure is valid provided that $\delta\Psi = 0$ on C. Therefore, the choice of a trial function must be such that this condition is satisfied. As will be seen, it is not a particularly restrictive requirement, and it is compatible with a number of trial functions that would seem to be acceptable in their simplicity and possible resemblance to an exact solution to equation (3).

Here two very simple trial functions will be chosen on an experimental basis, the first derived from the very low frequency solution to (3) for a circular tube, and the second an idealizaton of the high frequency solution. These trial functions will, therefore, be applicable, respectively, at low and high frequencies.

2.2.1. *Low frequencies*

In Figure 2 it is shown how the trial function $\tilde{\Psi}$ is defined at low frequencies. It is first assumed that there is one unique point O on R at which $\tilde{\Psi}$ has a maximum value and, moreover, that $\tilde{\Psi}$ decreases monotonically in a radial direction from O to C. The cross-section is then split up into a series of triangular regions (shown in Figure 2(a)), each of which has a vertex at O. The opposite side of each triangle forms a line segment ΔC which becomes a part of a polygonal approximation to the boundary C. One such triangle, with a co-ordinate s in the direction normal to ΔC, and having its origin at O, is shown in Figure 2(b). The distance from O to ΔC is L_i, and the area of the triangle is A_i. The number and arrangement of these triangles must be chosen so as to be compatible with the cross-sectional shape of the tube. For polygonal cross-sections, the number of triangles will be finite, but for more general curved shapes, it could be arbitrarily large. In practice, a reasonable approximation to the actual shape, by the juxtaposition of triangles, would suffice; an example of this is given later in this paper.

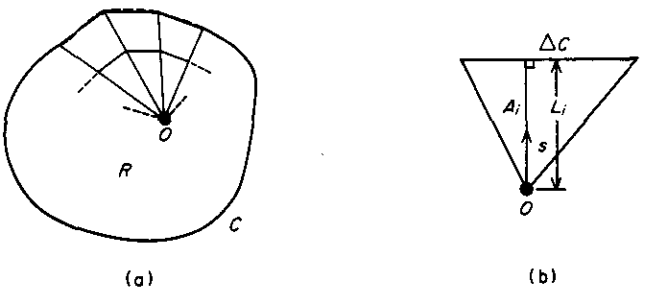

Figure 2. Low frequency trial function; (a) discretization of R; (b) a triangular sub-region of R.

The exact solution of equation (3) for a circular section tube, and numerical computations of the velocity field by Craggs and Hildebrandt [11] for rectangular and triangular sections, suggest that, at low frequencies, a simple approximation to the true distribution of Ψ on R is such that lines of constant Ψ would run parallel to ΔC. Thus one would have $\tilde{\Psi} \equiv \tilde{\Psi}(\zeta)$, where $\zeta = s/L_i$; clearly, $\nabla\tilde{\Psi}$ will be parallel to the direction of the co-ordinate s. The exact solution for a circular tube, in the low frequency limit, has a parabolic radial variation of Ψ (cf. Poiseuille flow), and therefore one may choose

$$\tilde{\Psi} = \tilde{\Psi}_o(1 - \zeta^2) \tag{7}$$

as the radial dependence of $\tilde{\Psi}$ in the low-frequency trial function; here, $\tilde{\Psi}_o$ is the value of $\tilde{\Psi}$ at O. Note, at this point, that finding $\delta\tilde{\Psi}$ simply involves taking $\partial\tilde{\Psi}/\partial\tilde{\Psi}_o$; this derivative is zero everywhere on C, as is obvious from equation (7), so the aforementioned requirement concerning the application of the forced boundary condition is met.

Finding the location of O in a tube of arbitrary cross-section presents a problem. In the case of cross-sectional shapes having rotational symmetry (such as regular polygons, rectangles and ellipses), O would generally be located at the centroid of the R, but in the case of irregular figures (for example, right-angled triangles), the situation is less clear. Here one can have recourse again to the calculations of Craggs and Hildebrandt [11], who presented particle velocity contours in tubes having a right-angled triangular section. Their data at low frequencies indicate that O is located close to a point equidistant from the three sides of the triangle, that is, at the centre of the inscribed circle. This can be taken as a "rule of thumb" in the present case, although clearly it is not possible to inscribe a circle in an irregular polygon having more than three sides, so that it touches all sides. One may suggest, however, that in such cases, the location of O may be determined by inscribing the *largest possible* circle. Otherwise the centroid of the area could, perhaps, be chosen.

By inserting the expression for $\tilde{\Psi}$ from equation (7) into equation (6) and integrating over A_i, one finds that the contribution to Φ from a single area element is

$$\Phi_i = (1/2)[\Psi_o^2 \Delta C/L_i + (i\omega/\eta)\Psi_o^2 A_i/3 - (i2\omega/\eta)\Psi_o A_i/2], \tag{8}$$

and, if one takes $\Phi = \sum_i \Phi_i$, it is clear that

$$\Phi(\Psi) = (1/2)\left(\Psi_o^2 \oint_C dC/L + i\omega\Psi_o^2 R/3\eta - i\omega\Psi_o R/\eta\right), \tag{9}$$

where L is just the normal distance from O to a line segment at any point (note that L can vary between area elements). Now, putting $\delta\Phi = 0$ simply involves equating $\partial\Phi/\partial\Psi_o$ to zero, and this yields

$$\Psi = (i\omega R/2\eta)\Big/\left[\oint_C dC/L + i\omega R/3\eta\right], \tag{10}$$

and, from the above definition of $F(\eta)$,

$$F(\eta) = \Psi_o/2 = (i\omega R/4\eta)\Big/\left[\oint_C dC/L + i\omega R/3\eta\right]. \tag{11}$$

It is evident that the integral in equations (10) and (11) can be evaluated for a continuously curved boundary C (which can be viewed as a series of infinitesimally short line segments) such as a circle, or for a polygonal shape such as a triangle or a pentagon. Equation (11) may be used in conjunction with equation (4) to find the axial attenuation rate and phase speed of the wave at low frequencies in a tube of arbitrary cross-sectional shape. One obvious limitation of the present approach is that, if L becomes less than zero, then the trial function—as defined above—ceases to have any meaning; however, this should not prove unduly restrictive in most cases of interest.

If the cross-sectional shape is a regular polygon, the length L is simply the hydraulic radius of the cross-section, r_h (equal to twice the area divided by the perimeter). It is clear in this case that $R = r_h C/2$ and $\oint_C dC/L = C/r_h$. Then equation (11) becomes

$$F(\eta) = (i\omega r_h^2/4\eta)/[2 + i\omega r_h^2/3\eta]. \tag{12}$$

If the shape is not a regular polygon then, of course, L varies between area elements and cannot be identified with the hydraulic radius. According to the present model, therefore, the hydraulic radius is a useful parameter only in the case of a regular polygonal cross-section.

The low frequency model should be applicable up to a frequency at which the viscous or thermal boundary layer thickness (whichever is the smaller) becomes equal to the largest value of L (which we will denote L_{max}). The boundary layer thicknesses are given by the expressions

viscous: $$\delta_v = (2\nu/\omega)^{1/2}, \tag{13a}$$

thermal: $$\delta_t = (2\nu/\omega Pr)^{1/2} \tag{13b}$$

(see the book by Morse and Ingård [16], p. 286) and so the upper limiting frequency of the low frequency model is given by

$$f_1 = \min\,(\nu/\pi L_{max}^2,\ \nu/\pi L_{max}^2 Pr). \tag{14}$$

2.2.2. *High frequencies*

Both the exact solution for a circular tube and the numerical data of Craggs and Hildebrandt [11] indicate that, at high frequencies, the solution of equation (3) predicts roughly constant values of Ψ in the central region of the tube, with a fairly rapid fall-off to zero as the wall is approached in the boundary layer region. Typically, there is also an "overshoot" region just outside the boundary layer. An idealizaton of this sort of profile, which may be employed as the trial function, has a constant value of $\tilde{\Psi}(=\tilde{\Psi}_o)$ in the central region, with a linear decrease of $\tilde{\Psi}$ from the limit of the boundary layer to the

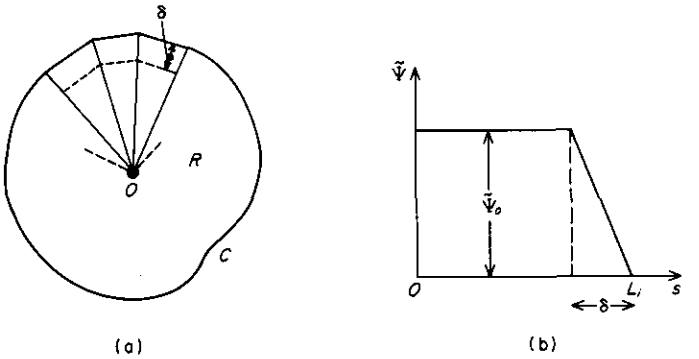

Figure 3. High frequency trial function; (a) discretization of R; (b) form of the assumed trial function.

wall. One again can split up the area R into discrete triangular regions, as shown in Figure (3a). The central point O is the same as that in the low frequency model. The assumed dependence of $\tilde{\Psi}$ on s is shown in Figure (3b); here, the boundary layer thickness δ is equal to δ_v or δ_t, as appropriate.

Now one finds (as in the case of equation (8)) that the contribution to Φ from a single element is

$$\Phi_i = (1/2)[\tilde{\Psi}_o^2 A_i(2\varepsilon_i - \varepsilon_i^2)/\delta^2 + (i\omega/\eta)\tilde{\Psi}_o^2 A_i(1 - 4\varepsilon_i/3 + \varepsilon_i^2/2) - (i2\omega/\eta)\tilde{\Psi}_o A_i(1 - \varepsilon_i + \varepsilon_i^2/3)], \tag{15}$$

where $\varepsilon_i = \delta/L_i$, and, *a priori*,

$$\Phi(\Psi) = (1/2)[\tilde{\Psi}_o^2 I_1/\delta^2 + (i\omega/\eta)\tilde{\Psi}_o^2 I_2 - (i2\omega/\eta)\tilde{\Psi}_o I_3], \tag{16}$$

where

$$I_1 = \oint_C (\delta - \delta^2/2L)\mathrm{d}C, \qquad I_2 = \oint_C (L/2 - 2\delta/3 + \delta^2/4L)\,\mathrm{d}C, \tag{17a, b}$$

$$I_3 = \oint_C (L/2 - \delta/2 + \delta^2/6L)\,\mathrm{d}C. \tag{17c}$$

Putting $\delta\Phi = 0$ yields, in this case,

$$\tilde{\Psi}_o = (\mathrm{i}\omega/\eta)I_3/[I_1/\delta^2 + (\mathrm{i}\omega/\eta)I_2] \qquad \text{and} \qquad F(\eta) = (\mathrm{i}\omega/\eta R)I_3^2/[I_1/\delta^2 + (\mathrm{i}\omega/\eta)I_2]. \tag{18a, b}$$

Equation (18b) may be used in the same way as equation (11) to find the axial attenuation rate and phase speed of the wave in the tube. In cases where the cross-section is a regular polygon, one may define a quantity $\varepsilon = \delta/L = \delta/r_h$ and also note that $\delta^2 = 2\eta/\omega$ (see equations (13a, b)); now, equation (18b) becomes

$$F(\eta) = \mathrm{i}2(1 - \varepsilon + \varepsilon^2/3)^2/[(2\varepsilon - \varepsilon^2) + \mathrm{i}2(1 - 4\varepsilon/3 + \varepsilon^2/2)]. \tag{19}$$

The high frequency model should be valid at frequencies above a limit f_2, at which the viscous or thermal boundary layer thickness (whichever is the larger) is equal to the smallest value of L (which we shall call L_{min}). Therefore

$$f_2 = \max\,(\nu/\pi L_{min}^2,\ \nu/\pi L_{min}^2 Pr). \tag{20}$$

3. RESULTS

In this section predictions made by the present method are to be compared to those based on other published work, for several cross-section geometries. It will be possible to assess the accuracy of the variational method, implemented by the use of the above trial functions, and to offer comments about other methods of solution. One example of an irregular cross-sectional geometry will also be described.

3.1. COMPARISON BETWEEN PREDICTIONS FOR VARIOUS GEOMETRIES

3.1.1. *A circular tube*

The classical case of the circular tube is the obvious choice for initial comparisons. Here, the radius a is equal to r_h in equation (12), and one has

$$F(\eta) = (\mathrm{i}\omega a^2/4\eta)/(2 + \mathrm{i}\omega a^2/3\eta) \tag{21}$$

as the low frequency variational solution, the high frequency solution being given by equation (19), with $\varepsilon = \delta/a$.

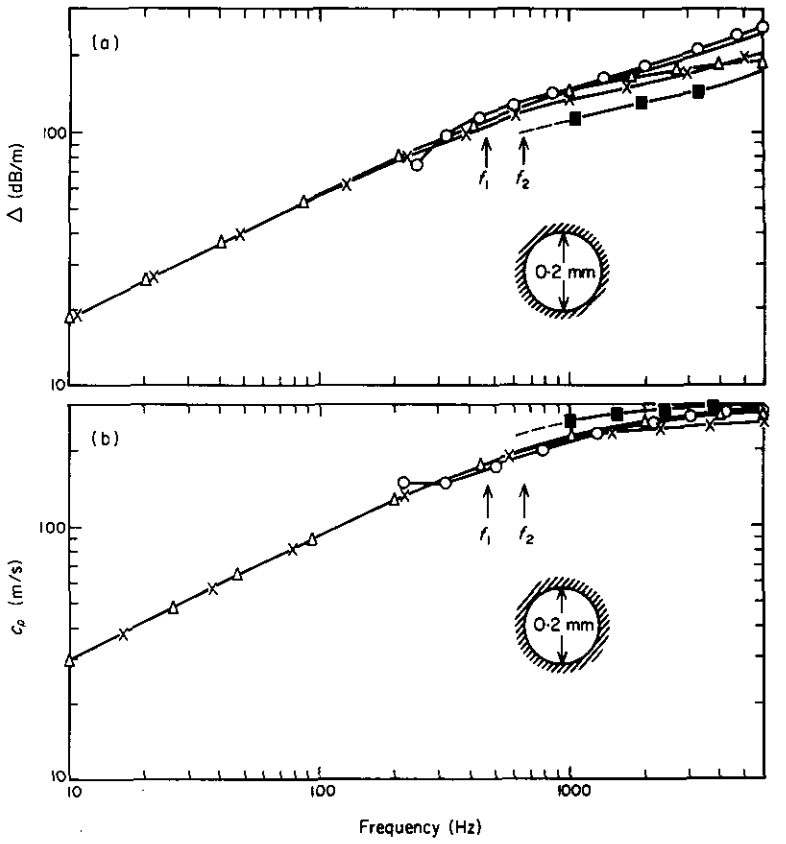

Figure 4. Axial attenuation rate and phase speed in a circular tube of 0·2 mm diameter; (a) attenuation rate, Δ; (b) phase speed, c_p; ——, exact solution (Stinson [13]); △—△, low frequency variational solution (equation (21)); ○—○, high frequency variational solution (equation (19)); ×—×, ■—■, isothermal, adiabatic numerical solution (Craggs and Hildebrandt [11, 12]).

In Figure 4(a) are shown plots of the axial attenuation rate, based on the present low frequency and high frequency models, together with the exact solution (see, for example, that of Stinson [13]) and the numerical results of Craggs and Hildebrandt [11, 12] for isothermal and adiabatic processes. The tube is 0·2 mm in diameter and contains air at 20°C (it is assumed that $\bar{\rho} = 1{\cdot}2\ \text{kg/m}^3$, $c = 344$ m/s, $\gamma = 1.4$, $\nu = 1{\cdot}5 \times 10^{-5}\ \text{m}^2/\text{s}$ and $Pr = 0{\cdot}71$). At frequencies up to 200 Hz, all methods agree closely in predicting Δ (except, of course, the high frequency variational curve, which is valid only above f_2, and the adiabatic data of Craggs and Hildebrandt, which would not be valid except at high frequencies). Above this frequency, the Craggs and Hildebrandt isothermal curve falls below the exact solution, presumably because the imaginary part of the effective fluid compressibility becomes significantly large, causing the isothermal assumption to break down. The adiabatic solution of Craggs and Hildebrandt is in even poorer agreement with the exact solution than the isothermal solution, though presumably at extremely high frequencies (beyond the range of the data presented in references [11, 12]) it should agree better. Above 1 kHz, the low frequency variational solution begins to give rather inaccurate results (as expected), but the high frequency solution is in quite good agreement with the exact solution.

The calculated phase speed is shown in Figure 4(b). All methods except the high frequency variational solution and the Craggs and Hildebrandt adiabatic solution agree very closely up to about 800 Hz, above which frequency the Craggs and Hildebrandt

isothermal predictions are low compared to the exact solution; their adiabatic predictions give results that are too high, although the trend is toward better agreement as the frequency increases. The low frequency variational solution gives quite good results for c_p, even up to 6 kHz (well above f_1, the notional upper frequency of validity). The high frequency variational solution agrees well with the exact solution above about 300 Hz and the agreement improves at higher frequencies.

3.1.2. *A parallel slit*

A slit with parallel walls has a suitably simple geometry for further comparison between theories; moreover, Attenborough [7] has considered the parallel slit and the circular tube as extremes of cross-sectional shape and for this reason too some attention should be devoted here to the slit. Clearly, the trial function proposed in section 2.2.1 is not appropriate in this case, and instead one can simply employ a parabolic function, which has the same form as the quasi-steady laminar flow solution for the velocity field or the very low frequency solution for temperature fluctuations. Following a process analogous to that given in equations (6)–(11) yields

$$F(\eta) = (i\omega a^2/12\eta)/(1 + i\omega a^2/10\eta) \tag{22a}$$

(a being, in this case, the width of the slit) for the low frequency variational solution and, in the high frequency case, the aforementioned linear boundary-layer profiles on both walls give the result

$$F(\eta) = i(1-\varepsilon)^2/[\varepsilon + i(1 - 4\varepsilon/3)], \tag{22b}$$

where $\varepsilon = \delta/a$.

In Figure 5, the axial attenuation rate in a slit 0·2 mm wide, calculated from the exact expression [7, 13] is compared with those from the low frequency and high frequency variational solutions (Craggs and Hildebrandt [11, 12] also computed data for a slit, but these are not shown here). The fluid properties have the above values. Up to 1 kHz, the low frequency curve is in close agreement with the exact solution, but falls below it above this frequency. At and above 1 kHz, the high frequency curve is in good agreement with the exact solution, although at lower frequencies, agreement is poorer; at $f = f_2$, for example, the variational solution overpredicts the attenuation by 8%.

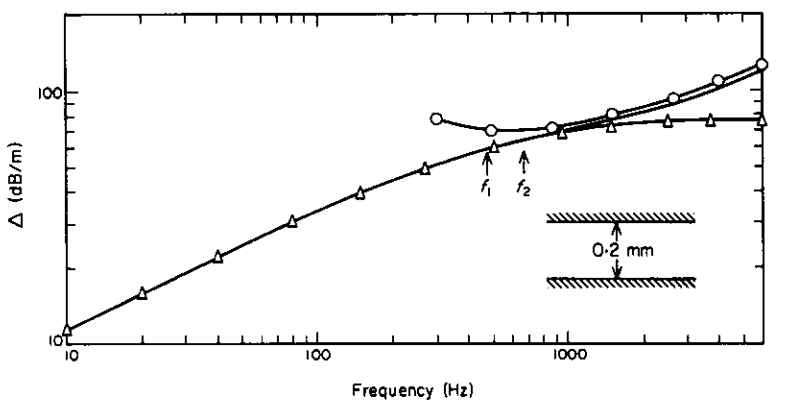

Figure 5. Axial attenuation rate, Δ, in a uniform slit of width 0·2 mm; ——, exact solution (Attenborough [7], Stinson [13]); Δ—Δ, low frequency variational solution (equation (22a)); O—O, high frequency variational solution (equation (22b)).

3.1.3. *An equilateral triangular section tube*

This is another simple geometry, intermediate between the circular tube and the parallel slit. As previously mentioned, an exact solution for this case has been reported by Stinson and Champoux [9, 10], and Craggs and Hildebrandt [11, 12] have given numerical results; therefore comparison with the variational solution is appropriate for this shape too. In Figure 6, the variation of Δ with frequency is shown for a tube with a cross-sectional shape having a side of 0·2 mm. Only the isothermal results of Craggs and Hildebrandt are shown here, and they are very close to the exact solution of Stinson and Champoux at low frequencies, but give figures that are too low at higher frequencies, as in the case of the circular tube. The low frequency variational solution gives results that are about 11% too high over the whole frequency range, and the high frequency solution gives results that are rather close to—but a little greater than—those of the low frequency solution.

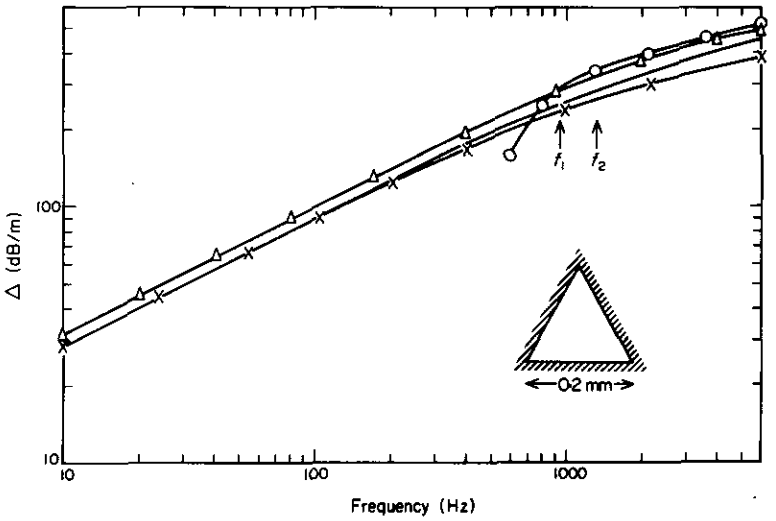

Figure 6. Axial attenuation rate, Δ, in an equilateral triangular section tube of side 0·2 mm; ——, exact solution (Stinson and Champoux [9, 10]); Δ—Δ, low frequency variational solution (equation (12)); O—O, high frequency variational solution (equation (19)); × — ×, numerical solution (Craggs and Hildebrandt [11, 12]).

Clearly, the variational solutions give results that—while being accurate within a reasonable margin—are inferior to those obtained in the cases of the circular tube and slit. This is, of course, because of the relative closeness with which the assumed trial functions resemble the exact solutions. The low frequency trial functions for the circular tube and slit have the same form as the solution for the velocity field in quasi-steady laminar flow or for very low frequency temperature fluctuations (see, for example, the paper by Stinson [13] for sample data on a circular tube), and therefore the corresponding variational solutions will certainly agree with the exact solutions at vanishingly low frequencies. On the other hand, the trial function for the triangular tube does not happen to coincide precisely with the actual steady flow solution (although this solution could have been extracted, if desired, from the acoustic solution of Stinson and Champoux [9, 10]). Consequently, the accuracy of the solution in the case of the triangular tube is somewhat degraded, and the only way in which it could be improved is for a more accurate trial function to be chosen. In Figure 7, the computed velocity pattern (taken from the results of Craggs and Hildebrandt [11]) in a tube having a right-angled isosceles triangular cross-section is compared to the low frequency trial function (no computed data having been

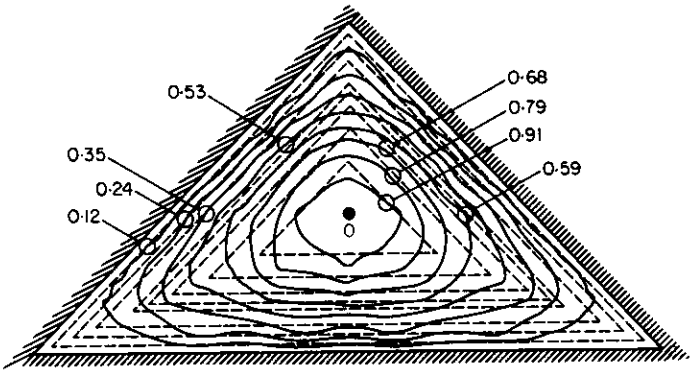

Figure 7. Comparison between the low frequency trial function, — —, and the computed axial particle velocity contours of Craggs and Hildebrandt [11],——, for an isosceles right-angled triangular section tube with $r_h(\bar{\rho}\omega/\mu)^{1/2}=0{\cdot}01$.

given in reference [11] for an equilateral triangle). The frequency is low here, and a frequency parameter equal to $r_h(\bar{\rho}\omega/\mu)^{1/2}$ has a value of 0·01 for these data; it is the real part of the particle velocity that is shown (the imaginary part, out of phase with the pressure, being five orders of magnitude less than the real part), and contours of relative axial velocity are plotted; these are labelled with numerical values, 1·0 corresponding to the velocity at O. It can immediately be seen that although the trial function is broadly consistent with the computed velocity pattern the sharp corners of the assumed contours do not appear in the computed curves, particularly towards the centre of the tube (near the sides, the agreement is better). However, this disparity is not as severe as it might seem, because it is more important for the trial function to be close to the actual velocity pattern near the walls (where the transverse velocity gradient is greatest) than near the centre. Nonetheless, differences of this sort do account for the discrepancies noted in Figure 6, between the variational and exact solutions for the equilateral triangular tube. The slight overprediction of attenuation, by the variational method, may be explained by the assumption of a constant wall shear stress along each wall, whereas a fall-off towards the corners is evident in the numerical solution.

3.1.4. *A square section tube*

The series solution of Roh *et al.* [8] for a rectangular tube yields the expression

$$F(\eta)=(4\mathrm{i}\omega/\eta b^2h^2)\sum_{j=0}^{\infty}\sum_{k=0}^{\infty}[\alpha_j^2\beta_k^2(\alpha_j^2+\beta_k^2+\mathrm{i}\omega/\eta)]^{-1} \tag{23}$$

(see the paper by Stinson [13]); here, b and h are the lengths of the sides of the cross-section and

$$\alpha_j=(j+1/2)\pi/b, \qquad \beta_k=(k+1/2)\pi/h. \tag{24a, b}$$

In Figure 8 are shown results from equations (23) and (24), for Δ in a square tube of side 0·2 mm, plotted against the variational solutions for low and high frequencies and the (isothermal) numerical solution of Craggs and Hildebrandt [11, 12]. The comparison is qualitatively similar to that for the equilateral triangle, although the low frequency variational solution fares rather better in this case, where the internal angles of the polygonal cross-section are greater. One can infer that the assumed trial function is rather closer to reality for a square cross-section than for an equilateral triangle. The high frequency variational solution gives predictions about 10% too great. As expected, the Craggs and

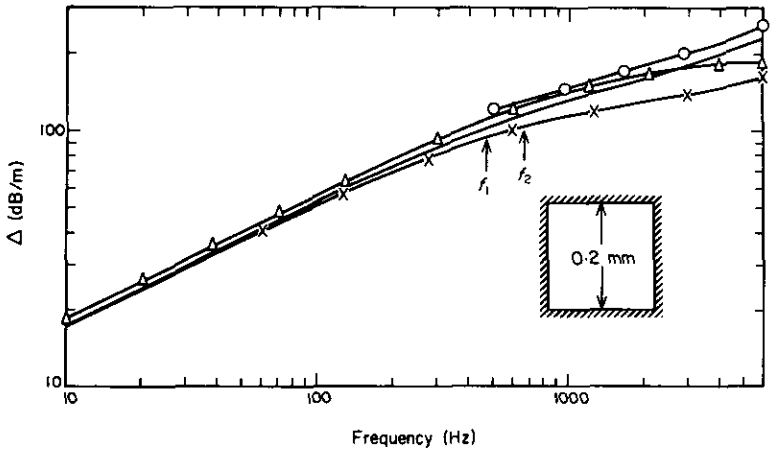

Figure 8. Axial attenuation rate, Δ, in a square section tube of side 0.2 mm; ——, exact solution (Roh *et al.* [8]); Δ—Δ, low frequency variational solution (equation (12)); O—O, high frequency variational solution (equation (19)); ×—×, numerical solution (Craggs and Hildebrandt [11, 12]).

Hildebrandt figures virtually coincide with the exact solution at low frequencies, but give results that are too low at high frequencies.

3.1.5. *A rectangular section tube*

Curves of Δ for a tube of rectangular cross-section, measuring 0·2 mm × 0·5 mm, are plotted in Figure 9. Only the exact solution of Roh *et al.* [8] and the low frequency and high frequency variational solutions (taken from equations (11) and (18b)) are shown. The variational solutions give results that are rather close to the exact solutions in this case, both at low and high frequencies. The exact solution for a slit 0·2 mm wide is also plotted up to 200 Hz, for comparison, and it can be seen that, with this larger aspect ratio (as compared to the square tube), the values of Δ for the rectangular tube begin to approach those for the slit. Craggs and Hildebrandt [11] have carried out a somewhat more detailed comparision for tubes of various aspect ratios and have reached similar conclusions.

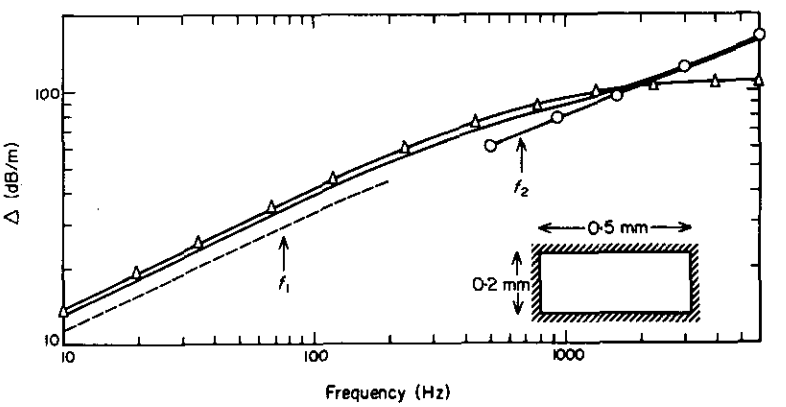

Figure 9. Axial attenuation rate, Δ, in a rectangular section tube of cross-sectional dimensions 0·2 mm × 0·5 mm; ——, exact solution (Roh *et al.* [8]); Δ—Δ, low frequency variational solution (equation (11)); O—O, high frequency variational solution (equation (18b)); — —, exact solution for a slit of width 0·2 mm (Attenborough [7], Stinson [13]).

3.1.6. *A hexagonal section tube*

The hexagon is a shape intermediate between the square and the circle, and Craggs and Hildebrandt [11] have given numerical computations of effective density and resistivity parameters which show that—as one would expect—these quantities, for a hexagonal section tube, fall between the values for square and circular section tubes. No exact solution for sound propagation in hexagonal tubes appears to have been reported, and the only valid comparison that can be made here is between the low frequency variational solution (equation (12)) and the data of Craggs and Hildebrandt with an isothermal effective sound speed [11, 12]. Acordingly, these two predictions are plotted in Figure 10, over the frequency range 1 – 1000 Hz. One can note very good agreement between the two methods up to 100 Hz, with small but increasing discrepancies from 300 Hz to 1 kHz. At higher frequencies, these discrepancies can be expected to be greater still.

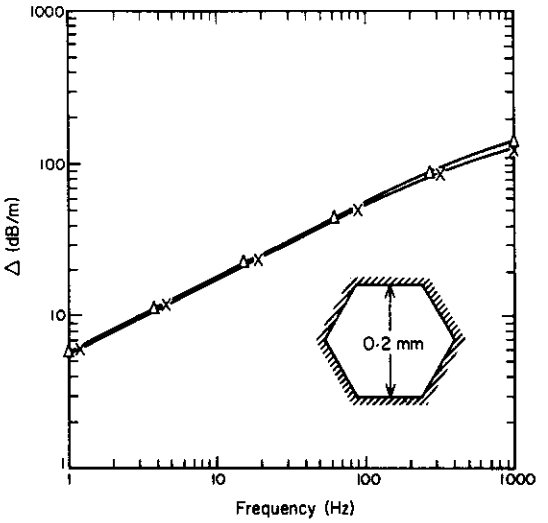

Figure 10. Axial attenuation rate, Δ, in a hexagonal section tube of width 0·2 mm; Δ—Δ, low frequency variational solution (equation (12)); ×—×, numerical solution (Craggs and Hildebrandt [11, 12]).

3.2. AN IRREGULAR GEOMETRY: THE SEMI-CIRCLE

It is instructive to examine one example of an irregular cross-sectional geometry, and the semi-circle would seem to be an appropriate shape. An exhaustive analysis is not presented here, but the discussion is restricted to the low frequency variational solution and this is used as a vehicle to illustrate how one can construct an appropriate trial function and formulate an expression for $F(\eta)$.

In Figure 11, a fairly simple way of dividing the area into triangular sub-regions is shown. The central point O is chosen to be mid-way along the axis of symmetry of the area, and the cross-section is slit up into seven sub-regions, as shown. This is probably the minimum number that would give acceptably accurate results. Taking a greater number of triangular sub-regions would probably not be advantageous in view of the likely limited resemblance between the trial function and the actual velocity and temperature fields.

With the radius of the semi-circle denoted by a, then by graphical or geometrical methods one can very simply determine the parameters R and $\oint_C \mathrm{d}C/L$ (see equation (11)). For the

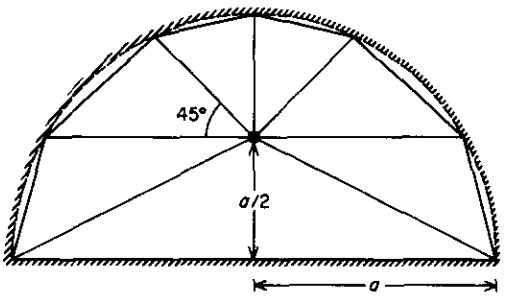

Figure 11. Triangular sub-regions for a semi-circular section tube.

chosen method of subdivision of the area, one finds

$$R = 1{\cdot}49\,a^2, \qquad \oint_C \mathrm{d}C/L = 9{\cdot}07. \tag{25a, b}$$

The expression for $F(\eta)$ obtained from equation (11) is therefore

$$F(\eta) = (0{\cdot}0822\,\mathrm{i}\omega a^2/\eta)/(2 + 0{\cdot}11\,\mathrm{i}\omega a^2/\eta). \tag{26a}$$

The hydraulic radius of the cross-section is equal to $a/(1+2/\pi)$, and use of equation (12) would give

$$F(\eta) = (0{\cdot}0933\,\mathrm{i}\omega a^2/\eta)/(2 + 0{\cdot}124\,\mathrm{i}\omega a^2/\eta). \tag{26b}$$

Equation (26b) is not really appropriate to an irregular cross-section such as this, but the discrepancies between the numerical values in equations (26a, b) are not very great.

3.3. ANALYSIS OF RESULTS

In the case of tubes having a regular polygonal cross-section, the low frequency and high frequency variational solutions—resulting from the assumed trial functions—give particularly simple low frequency and high frequency formulae for $F(\eta)$, viz., equations (12) and (19), and these are *both* expressed in terms of the hydraulic radius of the cross-section. This is, of course, a consequence of the assumed forms of the low frequency and high frequency trial functions. For this reason too, the hydraulic radius ceases to be a useful parameter for tubes that have cross-sections that are not regular polygons (as explained in section 2.2.1) and the slit, and the rectangular tube with an aspect ratio different from unity, would fall into this category; even so, very simple expressions exist for $F(\eta)$ at low and high frequencies in these other cases. It is worth noting that, in the present method, there is no need for a "shape factor" (as described by Attenborough [7] and Stinson and Champoux [13], and defined in terms of the steady flow resistance per unit length of the tube) that is used when circular tube results are applied to non-circular geometries.

It is of interest to compare the low frequency variational solutions for the circle and slit (the extremes of geometry) to the exact solutions. The circular tube solution for $F(\eta)$ is (see reference [13])

$$F(\eta) = 1 - 2\mathrm{J}_1[a(-\mathrm{i}\omega/\eta)^{1/2}]/a(-\mathrm{i}\omega/\eta)^{1/2}\mathrm{J}_0[a(-\mathrm{i}\omega/\eta)^{1/2}], \tag{27}$$

where $\mathrm{J}_0(\,\cdot\,)$ and $\mathrm{J}_1(\,\cdot\,)$ are Bessel functions of the first kind. Equations (21) and (27) may

be expanded in $a(\omega/\eta)^{1/2}$, and both give identical results up to the second term,

$$F(\eta) = i\omega a^2/8\eta + \omega^2 a^4/48\eta^2 + \cdots . \tag{28}$$

The criterion expressed in equation (14) is equivalent to $a(\omega/\eta)^{1/2} \leqslant \sqrt{2}$, and therefore the low frequency variational solution should be accurate at frequencies where this inequality holds. The exact solution for the case of the slit (see, for example, reference [13]) is

$$F(\eta) = 1 - \tanh\,[a(i\omega/4\eta)^{1/2}]/a(i\omega/4\eta)^{1/2} \tag{29}$$

(a being, in this case, the width of the slit). Equations (22a) and (29) may be expanded in $a(\omega/4\eta)^{1/2}$ and, as in the case of the circular tube, the results agree exactly up to the second term,

$$F(\eta) = i\omega a^2/12\eta + \omega^2 a^4/120\eta^2 + \cdots . \tag{30}$$

An accuracy criterion similar to that above will hold here, where the viscous or thermal boundary-layer thickness (whichever is the smaller) is greater than or equal to the semi-width of the slit. The good agreement between the variational and exact solutions, at low frequencies, for the circle and the slit is obtained because (as previously mentioned) the trial functions have the same forms as the very low frequency solutions to the velocity and temperature fields. One would not see such close correspondence in the cases of equilateral triangular or rectangular section tubes.

4. DISCUSSION

It has been shown here that a variational approach to the problem of sound propagation in uniform tubes of arbitrary cross-section can provide a very simple method of approximate solution which gives results of acceptable accuracy in comparison with exact or numerical solutions. One appealing feature of this type of method is that there is considerable scope for improvement in the results, by the choice of more versatile trial functions that can more nearly approach the true solutions to the governing equations. This can, for example, be done by the use of multiple-degree-of-freedom trial functions: that is, the solution region can be split up into separate areas, *each* with its own trial function involving unknown coefficients (in contrast to the foregoing, where—although the cross-section is divided into sub-regions—there is only one unknown coefficient, and the trial functions for the component areas all have the same form). The sub-regions between the vertices of a polygonal region and the centre could, perhaps, be treated separately from the rest of the region. Equating the variation of the functional (expressed, piecewise, as the sum of integrals over the various sub-regions) to zero would then involve taking partial derivatives of the functional, with respect to the unknown coefficients, and equating these derivatives separately to zero, giving rise to a system of homogeneous linear equations. The resulting determinantal equation would then be the disperson equation for the waves, and could be solved analytically or numerically, depending on its complexity. Of course, there comes a point, in this method of treatment, at which the number of sub-regions is sufficiently great to render the method excessively cumbersome. In this case, a finite element treatment could be used instead.

It was not considered appropriate, in the present investigation, to pursue this question of more elaborate trial functions, although there may well be some point in doing so, should the occasion demand. Rather, the object was to present an alternative to exact or purely numerical solutions and to suggest a framework for possible further development.

The simplicity of the approximate solutions above would, of course, be lost with increasing refinement in the solution method.

The current understanding of sound propagation in uniform tubes of arbitrary cross-section is probably sufficiently well developed that any future effort in this direction might be better devoted to other aspects of porous media, such as investigation of the effects of pore size distribution [17] and non-uniformity of pore cross-sectional area (Stinson and Champoux [10] are evidently currently examining this problem). These comments apply to porous media without any internal mean flow. The catalytic converters that are now often fitted to automobile exhaust systems usually incorporate laminar mean flows in polygonal (often square) section tubes; even assuming a constant temperature, one would almost certainly need to resort to numerical solution methods in order to model the acoustics of such systems adequately. Of course, taking account of the inevitable temperature gradients would introduce further complications.

REFERENCES

1. G. KIRCHHOFF 1868 *Annalen der Physik und Chemie* **134**, 177–193. Ueber den Einfluss der Wärmeleitung in einem Gase auf die Schallbewegung.
2. J. W. STRUTT (LORD RAYLEIGH) 1945 *Theory of Sound* (second edition, two volumes). New York: Dover Publications. See Vol. II, pp. 319–333.
3. C. ZWIKKER and C. W. KOSTEN 1949 *Sound Absorbing Materials*. Amsterdam: Elsevier Press.
4. H. TIJDEMAN 1975 *Journal of Sound and Vibration* **39**, 1–33. On the propagation of sound waves in cylindrical tubes.
5. M. A. BIOT 1956 *Journal of the Acoustical Society of America* **28**, 179–191. Theory of propagation of elastic waves in a fluid-saturated porous solid. II. Higher frequency range.
6. P. G. SMITH and R. A. GREENKORN 1971 *Journal of the Acoustical Society of America* **52**, 247–253. Theory of acoustical wave propagation in porous media.
7. K. ATTENBOROUGH 1983 *Journal of the Acoustical Society of America* **73**, 785–799. Acoustical characteristics of rigid fibrous absorbents and granular materials.
8. H.-S. ROH, W. P. ARNOTT, J. M. SABATIER and R. RASPET 1991 *Journal of the Acoustical Society of America* **89**, 2617–2624. Measurement and calculation of acoustic propagation constants in arrays of small air-filled rectangular tubes.
9. M. R. STINSON and Y. CHAMPOUX 1990 *Paper presented at the 120th Meeting of the Acoustical Society of America, San Diego, California, 26–30 November* 1990. Assignment of shape factors for porous materials having simple pore geometries.
10. M. R. STINSON and Y. CHAMPOUX 1992 *Journal of the Acoustical Society of America* **91**, 685–695. Propagation of sound and the assignment of shape factors in model porous materials having simple pore geometries.
11. A. CRAGGS and J. G. HILDEBRANDT 1984 *Journal of Sound and Vibration* **92**, 321–331. Effective densities and resistivities for acoustic propagation in narrow tubes.
12. A CRAGGS and J. G. HILDEBRANDT 1986 *Journal of Sound and Vibration* **105**, 101–107. The normal incidence absorption coefficient of a matrix of narrow tubes with constant cross-section.
13. M. R. STINSON 1991 *Journal of the Acoustical Society of America* **89**, 550–558. The propagation of plane sound waves in narrow and wide circular tubes, and generalization to uniform tubes of arbitrary cross-sectional shape.
14. A. CUMMINGS and I.-J. CHANG 1987 *Journal of Sound and Vibration* **114**, 565–581. Acoustic propagation in porous media with internal mean flow.
15. O. C. ZIENKIEWICZ and R. L. TAYLOR 1990 *The Finite Element Method* (fourth edition), Volume 1. New York: McGraw-Hill. See Chapter 9.
16. P. M. MORSE and K. U. INGÅRD 1968 *Theoretical Acoustics*. New York: McGraw-Hill.
17. K. ATTENBOROUGH 1991 Personal communication.